Neutron matter, symmetry energy and neutron stars

S Gandolfi[1] and A W Steiner[2,3]

[1]Theoretical Division, Los Alamos National Laboratory, Los Alamos, New Mexico 87545, USA
[2]Department of Physics and Astronomy, University of Tennessee, Knoxville, Tennessee 37996, USA
[3]Physics Division, Oak Ridge National Laboratory, Oak Ridge, Tennessee 37831, USA

Abstract. Recent progress in quantum Monte Carlo with modern nucleon-nucleon interactions have enabled the successful description of properties of light nuclei and neutron-rich matter. Of particular interest is the nuclear symmetry energy, the energy cost of creating an isospin asymmetry, and its connection to the structure of neutron stars. Combining these advances with recent observations of neutron star masses and radii gives insight into the equation of state of neutron-rich matter near and above the saturation density. In particular, neutron star radius measurements constrain the derivative of the symmetry energy.

1. Introduction

In the last few decades, properties of nuclear systems have been successfully described by nucleon-nucleon potentials like Argonne and Urbana/Illinois forces, that reproduces two-body scattering and properties of light nuclei with very high precision [1, 2]. These nuclear potentials reproduce several properties of nuclear systems extremely well, including binding energies of ground- and excited states, radii, matrix elements, scattering states, and other observables [3, 4, 5, 6]. The Argonne AV18 nucleon-nucleon interaction has small non-local terms and a hard core. The use of correlated wave functions combined with Quantum Monte Carlo (QMC) methods has provided highly accurate solutions of the ground state of many-body nuclear systems [7].

The knowledge of the Equation of State (EoS) of pure neutron matter is an important bridge from the nucleon-nucleon interaction to neutron-rich matter. The symmetry energy $E_{\rm sym}$ is the difference of nuclear matter and neutron matter energy and gives the energy cost of the isospin-asymmetry in the homogeneous nucleonic matter. In the last few years the study of $E_{\rm sym}$ has received considerable attention (see for example Ref. [8] for a recent experimental/theoretical review). The role of the symmetry energy is essential to understand the mechanism of stability of very neutron-rich nuclei, and is also related to many phenomena occurring in neutron stars. The number of protons per baryon, x, is determined by beta-equilibrium and charge neutrality. These imply relationships between the chemical potentials and the symmetry energy, $\mu_e = \mu_n - \mu_p \approx 4E_{\rm sym}(1-2x)$. Matter near the nuclear saturation density is very neutron-rich, because electron degeneracy drives $\mu_n > \mu_p$. Thus neutron star matter is sensitive to $E_{\rm sym}$ and its first derivative. The inner crust of neutron stars, where the density is a fraction of nuclear densities, is mostly composed of neutrons surrounding a matter made of extremely-neutron rich nuclei that, depending on the density, may exhibit very different phases and properties. The extremely rich phase diagram of crustal matter is strongly related to the role of $E_{\rm sym}$. For

example, it governs the phase-transition between the crust and the core [9] and the nature of r-mode instabilities [10, 11].

2. The Nuclear Hamiltonian and Quantum Monte Carlo

In our model, neutrons are non-relativistic point-like particles interacting via two- and three-body forces:

$$H = \sum_{i=1}^{A} \frac{p_i^2}{2m} + \sum_{i<j} v_{ij} + \sum_{i<j<k} v_{ijk} \,. \tag{1}$$

The two body-potential that we use is the Argonne AV8′ [12], that is a simplified form of the Argonne AV18 [1]. Although simpler to use in QMC calculations, AV8′ provides almost the same accuracy as AV18 in fitting NN scattering data [13]. The three-body force is not as well constrained as the NN interaction, but its inclusion in realistic nuclear Hamiltonians is important to correctly describe the binding energy of light nuclei [2].

The Urbana IX (UIX) three-body force has been originally proposed in combination with the Argonne AV18 and AV8′ [14]. Although it slightly underbinds the energy of light nuclei, it has been extensively used to study the equation of state of nuclear and neutron matter [15, 16, 17]. The Illinois forces have been introduced to improve the description of both ground- and excited-states of light nuclei, showing an excellent accuracy [2, 3], but it produces an unphysical overbinding in pure neutron systems [18, 19].

Another interesting class of nucleon-nucleon potentials are derived within the chiral effective field theory. Typically, these interactions have strong non-local terms, and as a consequence they cannot be easily included in QMC calculations. Recently it has been showed that these potentials can be designed to be local, and combined with QMC simulations [20]. However, the need to include a cutoff to the nucleon's momentum limits the applicability of chiral forces to study dense neutron matter. The cutoff of these potentials can be controlled in a many-body calculation [20], but the uncertainty is already quite large at saturation density in neutron matter, making the calculation at larger densities unfeasible.

We solve the many-body ground-state with a projection in imaginary-time, i.e.:

$$\Psi(\tau) = \exp[-H\tau]\Psi_v \,, \tag{2}$$

where Ψ_v is a variational ansatz, and H is the Hamiltonian of the system. In the limit of $\tau \to \infty$, Ψ approaches the ground-state of H. The evolution in imaginary-time is performed by sampling configurations of the system using Monte Carlo techniques, and expectation values are evaluated over the sampled configurations. The main difference between GFMC and AFDMC is in the way that spin/isospin states are treated. In GFMC, all the spin/isospin states are explicitly included in the variational wave function. The results obtained are very accurate but limited to the ^{12}C [3] or 16 neutrons [21]. The AFDMC method samples the spin/isospin states using the Hubbard-Stratonovich transformation rather than simpling them explicitly [22]. The calculation can be then extended up to many neutrons, making the simulation of homogeneous matter and heavy nuclear systems possible [23]. The AFDMC has proven to be very accurate when compared to GFMC calculation of energies of neutrons confined in an external potential [21]. We shall present results obtained either using GFMC and AFDMC.

3. The Equation of State of Neutron Matter

In this section we present QMC results for pure neutron matter. There are several reasons to focus on pure neutron matter. First, the three-body interaction is non-zero only in the $T = 3/2$ isospin-channel (T is the total isospin of three-nucleons), while in the presence of protons there are also contributions in $T = 1/2$. The latter term is the dominant one in nuclei, and only

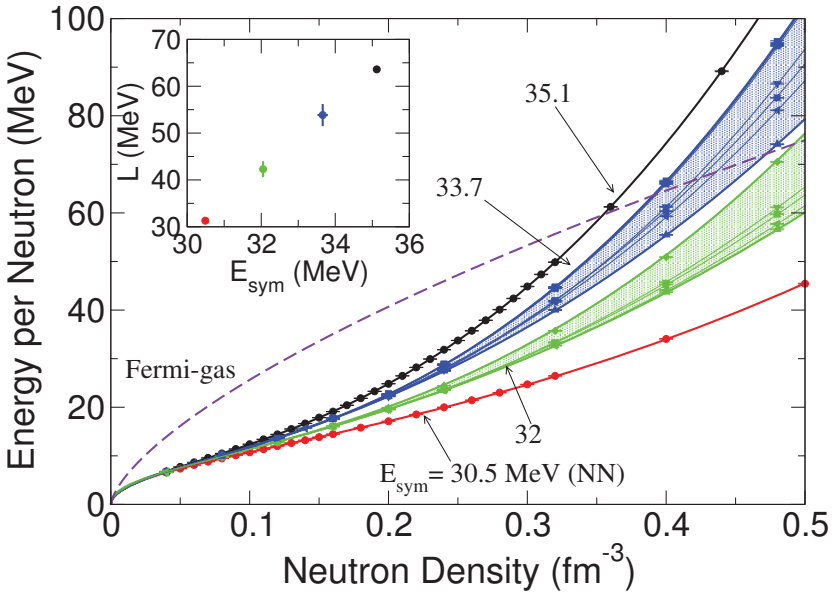

Figure 1. The QMC equation of state of neutron matter for various Hamiltonians. The red (lower) curve is obtained by including the NN (Argonne AV8′) alone in the calculation, and the black one is obtained by adding the Urbana IX three-body force. The green and blue bands correspond to EoSs giving the same $E_{\rm sym}$ (32 and 33.7 MeV respectively), and are obtained by using several models of three-neutron force. In the inset we show the value of L as a function of $E_{\rm sym}$ obtained by fitting the EoS. The figure is taken from Ref. [17].

weakly accessible by studying properties of nuclei. Second, the EoS of pure neutron matter is closely related to the structure of neutron stars.

We present several EoSs obtained using different models of three-neutron force in Fig. 1. The two solid lines correspond to the EoSs calculated using the NN potential alone and including the UIX three-body force [14]. The effect of using different models of three-neutron force is clear in the two bands, where the high density behavior is showed up to about $3\rho_0$. At such high density, the various models giving the same symmetry energy at saturation produce an uncertainty in the EoS of about 20 MeV. The EoS obtained using QMC can be conveniently fit using the following functional [16]:

$$E(\rho) = a\left(\frac{\rho}{\rho_0}\right)^{\alpha} + b\left(\frac{\rho}{\rho_0}\right)^{\beta}, \tag{3}$$

where E is the energy per neutron, $\rho_0 = 0.16$ fm^{-3}, and a, b, α and β are free parameters. The parametrizations of the EoS obtained from different nuclear Hamiltonians is given in Ref. [17].

At ρ_0 symmetric nuclear matter saturates, and we can extract the value of $E_{\rm sym}$ and L directly from the pure neutron matter EoS. The result of fitting the pure neutron matter EoS is shown in the inset of Fig. 1. The error bars are obtained by taking the maximum and minimum value of L for a given $E_{\rm sym}$, and the curves obtained with NN and NN+UIX are thus without error bars. From the plot it is clear that within the models we consider, the correlation between L and $E_{\rm sym}$ is linear and quite strong.

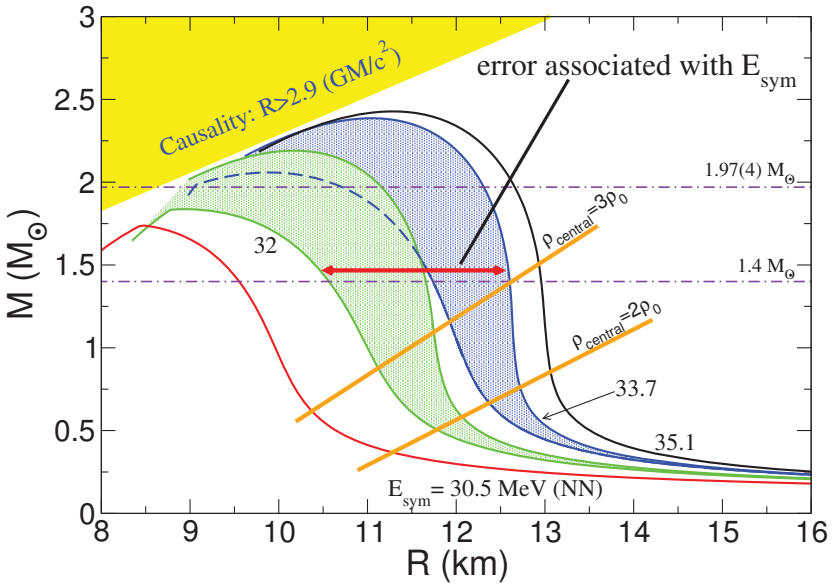

Figure 2. The mass-radius relation of neutron stars obtained from the EoS calculated using QMC. The various colors represent the $M - R$ result obtained from the corresponding EoSs described in Fig. 1. The two horizontal lines show the value of $M = 1.4$ and $1.97(4)M_\odot$ [24]. The figure is adapted from Ref. [17].

4. Connection to Neutron Star Masses and Radii

Neutron stars, unlike planets, are expected to be compositionally uniform, in which case their radius is determined principally by their mass; to a good approximation all neutron stars lie on a universal mass-radius $M-R$ curve. When the EoS of the neutron star matter has been specified, the structure of an idealized spherically-symmetric neutron star model can be calculated by integrating the Tolman-Oppenheimer-Volkoff (TOV) equations.

The neutron star mass measurements which provide the strongest EoS constraints are those which have the highest mass. Recent observations [24, 25] have found two neutron stars with masses near 2 $M_\odot$. These two data points provide some of the strongest constraints on the nature of zero-temperature QCD above the nuclear saturation density. We begin by examining what can be deduced about the M-R relation directly from these mass measurements, without employing a separate model for high-density matter. For lower densities we use the EoS of the crust obtained in Refs. [26] and [27]. For the core, we begin with the parameterization in Eq. 3, employing maximally stiff EoS when the QMC models violate the causality and become superluminal. The mass of a neutron star as a function of its radius is shown in Fig. 2. The two bands correspond to the result obtained using the two sets of EoS giving the same value of $E_{\rm sym}$ indicated in the figure. As in the case of the EoS, it is clear that the main source of uncertainty in the radius of a neutron star with $M = 1.4M_\odot$ is due to the uncertainty of $E_{\rm sym}$ rather than the model of the three-neutron force. The addition of a small proton fraction would change the radius R only slightly [28, 15], smaller than other uncertainties in the EoS that we have discussed. The numbers in the figure indicate the symmetry energy associated with the various equations of state. In the figure we also indicate with the orange lines the density of the neutron matter inside the star. Even at large masses the radius of the neutron star is mainly governed by the equation of state of neutron matter between 1 and 2 ρ_0 [29].

The AV8′ Hamiltonian alone does not support the recent observed neutron star with a mass

of $1.97(4)M_\odot$ [24]. However, adding a three-body force to AV8′ can provide sufficient repulsion to be consistent with all of the constraints [17]. There is a clear correlation between neutron star radii and the symmetry energy which determines the EoS of neutron matter between 1 and 2 ρ_0. The results in Fig. 2 also show that the most modern neutron matter EoS imply a maximum neutron star radius not larger than about 13 km, unless a drastic repulsion sets in just above the saturation density. This tends to rule out large values of L, typical of Walecka-type mean-field models without higher-order meson couplings which can decrease L.

5. Bayesian Analysis of Neutron Star Masses and Radii

In contrast to the mass measurements described above, neutron star radius measurements have proven more difficult, because they require both a distance measurement and some degree of modeling of the neutron star X-ray spectrum. Low-mass X-ray binaries (LMXBs) are neutron stars accreting matter from a low mass main-sequence or white dwarf companion. There are two types of LMXB observations which have recently provided neutron star radius information. The first type are LMXBs which exhibit photospheric radius expansion (PRE) X-ray bursts, thermonuclear explosions strong enough to temporarily lift the surface (photosphere) of the neutron star outwards [30, 31]. Several neutron stars have exhibited PRE X-ray bursts and four which have have been used to infer the neutron star mass and radius are given in the left panel of Fig. 3, using the methods described in Ref. [32]. The second type are quiescent LMXBs, (QLMXBs), where the accretion from the companion has stopped, allowing observation of the neutron star surface which has been heated by accretion [33]. A recent analysis of five neutron stars [34] including the possibility of both hydrogen and helium atmospheres and distance uncertainties is shown in the right panel of Fig. 3. Note that already from these two figures alone, it is clear that these probability distributions favor neutron star radii near 11 km. Although we will similar (R, M) distributions in our analysis below, it is important to remember that there are several systematic uncertainties which are potentially important. For the QLMXBs, the treatment of the X-ray absorption between the source and the observer, the flux calibration of the observing satellite, and the method used to measure the distance all play important roles. The situation for PRE X-ray bursts is even more challenging: complications such as spherical asymmetry, the time evolution of the spectra, and the location of the photosphere at "touchdown" may all modify the implied masses and radii.

Our goal is to constrain the EoS observational data described above, including the possibility of phase transitions in matter above the nuclear saturation density. In order to do this, we parametrize the EoS of matter at higher densities with a simple expression rich enough to include exotic matter. We perform a Bayesian analysis using data from QLMXBs and neutron stars which exhibit PRE bursts, where our model space is given by the EoS parameters and also one parameter for the mass of each neutron star in the data set. Given an EoS, the TOV equations provide the M-R curve and thus a prediction for the radius of each neutron star from its mass. As described above, we always ensure that our EoS are causal, hydrodynamically stable, and that our M-R curves support a 2 $M_\odot$ neutron stars. For densities near the saturation density, we an EOS parametrized in terms of the symmetry energy and compressibility. At higher densities, we describe matter either in terms of polytropes of the form $P = K_1\epsilon^\Gamma$, line-segments in the $P-\epsilon$ plane, or a simple parameterization of quark matter. The final results for the $M-R$ curve and EoS are given in Fig. 4 from Ref. [35]. The $M-R$ curve obtained is relatively vertical, which naturally implies that almost all neutron stars have approximately the same radius. The EoS obtained from the mass and radius observations is also in concordance with results from quantum Monte Carlo and chiral effective theory described above and constraints obtained from heavy-ion collisions.

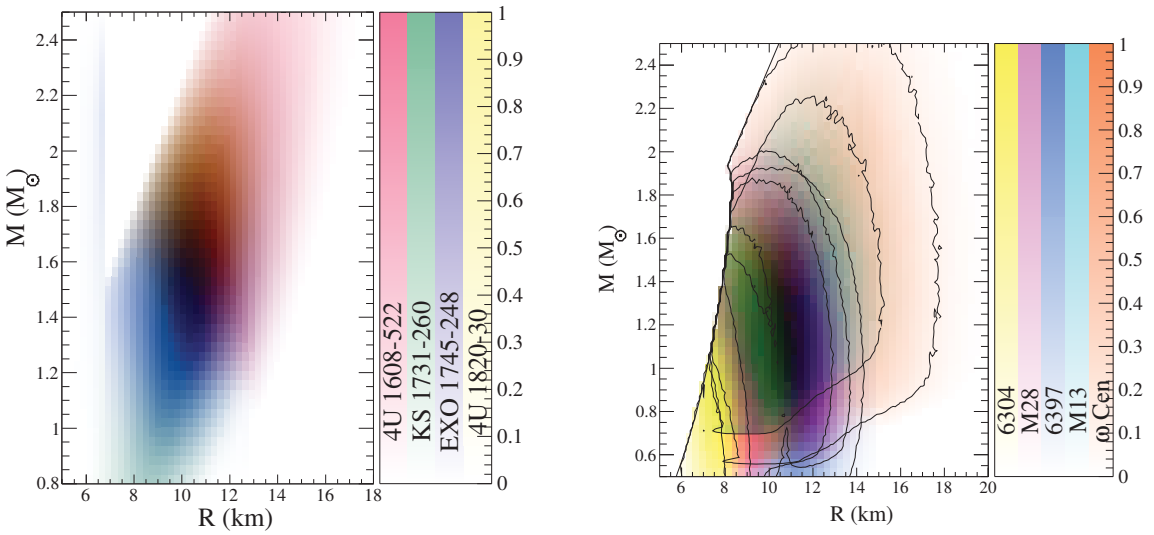

Figure 3. Left panel: Probability distributions in the mass-radius plane for four neutron stars exhibiting PRE X-ray bursts. Colors are added together in RGB color space. Right panel: Probability distributions in the mass-radius plane for five neutron stars in five globular clusters from Ref. [34]. Colors are added together in RGB color space when necessary. The contour lines outline the 90% confidence regions.

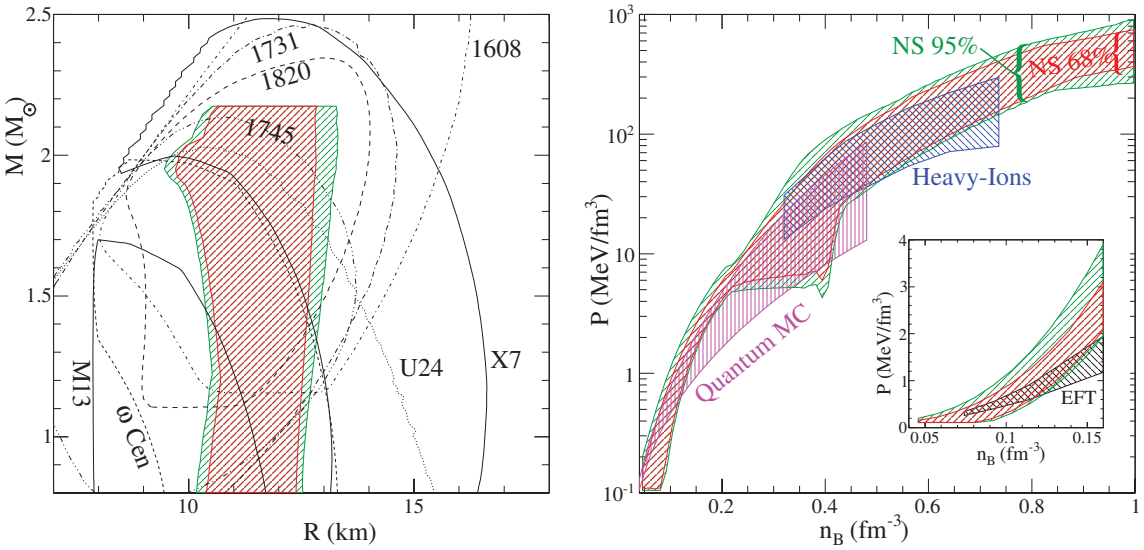

Figure 4. (Left panel) A comparison of the predicted M–R relation with the observations. The shaded regions outline the 68% and 95% confidences for the M–R relation. (Right panel) The predicted pressure as a function of baryon density of neutron-star matter as obtained from astrophysical observations. The region labeled "NS 68%" gives the 68% confidence limits and the region labeled "NS 95 %" gives the 95% confidence limits. Results for neutron-star matter from effective field theory [36] (see inset), from quantum Monte Carlo [17], and from constraints inferred from heavy-ion collisions [37] are also shown for comparison.

6. Determining the Density Dependence of the Symmetry Energy

In order to determine the symmetry energy, we use the parameterization of the neutron matter EoS from the quantum Monte Carlo results in Eq. 3 above. With this parameterization the symmetry energy at the saturation density $E_{\rm sym}$ and the parameter which describes the density dependence of the symmetry energy, L, are given by

$$E_{\rm sym} = a + b + 16\,, \quad L = 3\,(a\alpha + b\beta)\,. \tag{4}$$

Neutron stars contain a small amount of protons, so we multiply the EoS by a small ($\sim 10\%$) and density-dependent correction factor which modifies the pressure. This correction factor is obtained by averaging over Skyrme forces which give similar M-R curves to those suggested by the data.

While we do not obtain significant constraints on a or α, the mass and radius data do constrain the parameters b and β (Fig. 5). While the simple parametrization employed here cannot fully describe the complexities of the nuclear three-body force, it does make it clear that astrophysical data is beginning to rule out some three-body forces which might otherwise be acceptable. We also show constraints on L. From neutron stars we obtain the constraints to the symmetry energy and slope to be $32 < E_{\rm sym} < 34$ MeV and $43 < \mathrm{L} < 52$ MeV within 68% confidence. The only way to obtain a larger value of L is through a strong phase transition just above the nuclear saturation density which tends to decouple the properties of matter at low- and high-densities and allows for values of L as large as 83 MeV [35]. However, it is not clear that such a strong phase transition at low densities is particularly realistic, as it might have been already ruled out by experimental work in heavy-ion collisions as reviewed in Ref. [8].

7. Acknowledgements

SG is supported by the U.S. Department of Energy, Office of Nuclear Physics, by the NUCLEI SciDAC program and by the LANL LDRD program. AWS is supported by DOE Grant No. DE-FG02-00ER41132.

[1] Wiringa R B, Stoks V G J and Schiavilla R 1995 *Phys. Rev. C* **51** 38
[2] Pieper S C, Pandharipande V R, Wiringa R B and Carlson J 2001 *Phys. Rev. C* **64** 014001
[3] Pieper S C 2008 *AIP Conf. Proc.* **1011** 143
[4] Pieper S C and Wiringa R B 2001 *Annu. Rev. Nucl. Part. Sci.* **51** 53
[5] Nollett K M, Pieper S C, Wiringa R B, Carlson J and Hale G M 2007 *Phys. Rev. Lett.* **99**(2) 022502
[6] Schiavilla R, Wiringa R B, Pieper S C and Carlson J 2007 *Phys. Rev. Lett.* **98**(13) 132501
[7] Pudliner B S, Pandharipande V R, Carlson J, Pieper S C and Wiringa R B 1997 *Phys. Rev. C* **56** 1720
[8] Tsang M B, Stone J R, Camera F, Danielewicz P, Gandolfi S, Hebeler K, Horowitz C J, Lee J, Lynch W G, Kohley Z, Lemmon R, Möller P, Murakami T, Riordan S, Roca-Maza X, Sammarruca F, Steiner A W, Vidaña I and Yennello S J 2012 *Phys. Rev. C* **86** 015803
[9] Newton W G, Gearheart M and Li B A 2011 *arXiv:1110.4043* (*Preprint* `1110.4043`)
[10] Wen D H, Newton W G and Li B A 2012 *Phys. Rev. C* **85** 025801
[11] Vidaña I 2012 *Phys. Rev. C* **85** 045808
[12] Wiringa R B and Pieper S C 2002 *Phys. Rev. Lett.* **89** 182501
[13] Gandolfi S, Carlson J, Reddy S, Steiner A W and Wiringa R B 2013 *arXiv:1307.5815*
[14] Pudliner B S, Pandharipande V R, Carlson J and Wiringa R B 1995 *Phys. Rev. Lett.* **74** 4396
[15] Akmal A, Pandharipande V R and Ravenhall D G 1998 *Phys. Rev. C* **58** 1804
[16] Gandolfi S, Illarionov A Y, Schmidt K E, Pederiva F and Fantoni S 2009 *Phys. Rev. C* **79** 054005
[17] Gandolfi S, Carlson J and Reddy S 2012 *Phys. Rev. C* **85** 032801
[18] Sarsa A, Fantoni S, Schmidt K E and Pederiva F 2003 *Phys. Rev. C* **68** 024308
[19] Maris P, Vary J P, Gandolfi S, Carlson J and Pieper S C 2013 *Phys. Rev. C* **87**(5) 054318
[20] Gezerlis A, Tews I, Epelbaum E, Gandolfi S, Hebeler K, Nogga A and Schwenk A 2013 *Phys. Rev. Lett.* **111**(3) 032501
[21] Gandolfi S, Carlson J and Pieper S C 2011 *Phys. Rev. Lett.* **106** 012501
[22] Schmidt K E and Fantoni S 1999 *Phys. Lett. B* **446** 99
[23] Lonardoni D, Gandolfi S and Pederiva F 2013 *Phys. Rev. C* **87**(4) 041303

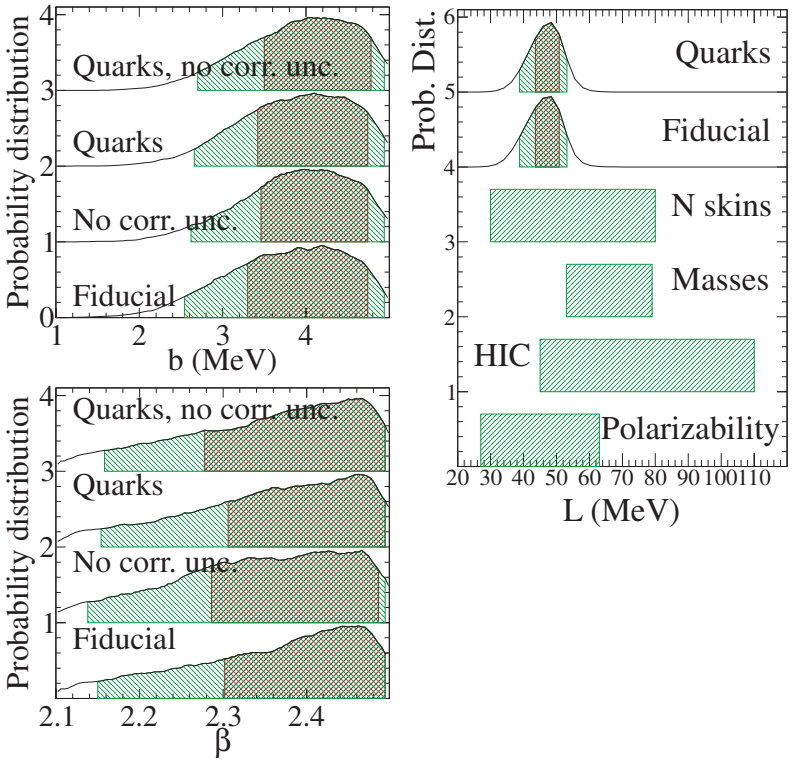

Figure 5. The left panel shows probability distributions of the parameters b and β obtained from the Bayesian analysis. The right panel summarizes constraints on L from observations and experiments. The top two curves show constraints on L as probability distributions assuming either the fiducial model of Ref. [38] or the model containing quarks. The bottom four curves show constraints on L from experiment, from neutron skins [39], nuclear masses [40], heavy-ion collisions [41], and from the electric dipole polarizability [42].

[24] Demorest P B, Pennucci T, Ransom S M, Roberts M S E and Hessels J W T 2010 *Nature* **467** 1081
[25] Antoniadis et al J 2013 *Science* **340** 448
[26] Baym G, Pethick C and Sutherland P 1971 *Astrophys. J.* **170** 299
[27] Negele J W and Vautherin D 1973 *Nucl. Phys. A* **207** 298
[28] Gandolfi S, Illarionov A Y, Fantoni S, Miller J, Pederiva F and Schmidt K 2010 *Mon. Not. R. Astron. Soc.* **404** L35
[29] Lattimer J M and Prakash M 2001 *Astrophys. J.* **550** 426
[30] van Paradijs J 1979 *Astrophys. J.* **234** 609
[31] Özel F, Baym G and Güver T 2010 *Phys. Rev. D* **82** 101301
[32] Steiner A W, Lattimer J M and Brown E F 2010 *Astrophys. J.* **722** 33
[33] Rutledge R, Bildsten L, Brown E, Pavlov G and Zavlin E 1999 *Astrophys. J.* **514** 945
[34] Lattimer J M and Steiner A W 2013 *arXiv:1305.3242*
[35] Steiner A W, Lattimer J M and Brown E F 2013 *Astrophys.J.* **765** L5
[36] Hebeler K and Schwenk A 2010 *Phys. Rev. C* **82** 014314
[37] Danielewicz P, Lacey R and Lynch W G 2002 *Science* **298** 1592
[38] Steiner A W and Gandolfi S 2012 *Phys. Rev. Lett.* **108** 081102
[39] Warda M, Viñas X, Roca-Maza X and Centelles M 2009 *Phys. Rev. C* **80** 024316
[40] Liu M, Wang N, Z-X L and Zhang F S 2010 *Phys. Rev. C* **82** 064306
[41] Tsang M B, Zhang Y, Danielewicz P, Famiano M, Li Z, Lynch W G and Steiner A W 2009 *Phys. Rev. Lett.* **102** 122701
[42] Tamii A, Poltoratska I, von Neumann-Cosel P, Fujita Y, Adachi T *et al.* 2011 *Phys. Rev. Lett.* **107** 062502